Corrin nitrogens and remote dimethylbenzimidazole nitrogen interactions in CObI(II)alamin studied with HYSCORE at X- and Q-band

ARTICLE *in* CHEMICAL PHYSICS LETTERS · MAY 2002

Impact Factor: 1.9 · DOI: 10.1016/S0009-2614(02)00521-3

24 May 2002

ELSEVIER

Chemical Physics Letters 358 (2002) 8–16

CHEMICAL PHYSICS LETTERS

www.elsevier.com/locate/cplett

Corrin nitrogens and remote dimethylbenzimidazole nitrogen interactions in Cob(II)alamin studied with HYSCORE at X- and Q-band

Jeffrey Harmer [b], Sabine Van Doorslaer [a], Igor Gromov [b], Arthur Schweiger [b,*]

[a] *Spectroscopy in Biophysics and Catalysis (SIBAC Laboratory), University of Antwerp, Universiteitsplein 1, 2610 Wilrijk, Belgium*
[b] *Lab. für Physikalische Chemie, Swiss Federal Institute of Technology, ETH Zurich, CH-8093 Zurich, Switzerland*

Received 8 March 2002

Abstract

A continuous wave and pulse electron paramagnetic resonance study of the base-on form of cob(II)alamin diluted in hydroxocob(III)alamin powder is presented. HYSCORE spectroscopy at X- and Q-band was used to study the weakly coupled corrin nitrogens and the remote nitrogen of the axial dimethylbenzimidazole ligand. Simulations of the spectra measured at different field positions enabled the following parameters to be determined; for the corrin nitrogens the hyperfine principal values are $A_1 = -4.5$ MHz, $A_2 = -3.4$ MHz and $A_3 = (-2.2$ to $-2.5)$ MHz with Euler angles $[\alpha, \beta, \gamma] = [n90, 25, 0]°$ and the nuclear quadrupole parameters are $e^2qQ/h = 1.75$ MHz and $\eta = 0.95$ with Euler angles $[\alpha, \beta, \gamma] = [90 + n90, 90, 12.5]°$, where $n = 0, 1, 2, 3$. The remote nitrogen of the dimethylbenzimidazole ligand has $A_1 = 1.75$ MHz, $A_2 = 1.75$ MHz and $A_3 = 2.10$ MHz with Euler angles $[\alpha, \beta, \gamma] = [-45, -10, 0]°$ and $e^2qQ/h = -3.3$ MHz and $\eta = 0.1$ with Euler angles $[\alpha, \beta, \gamma] = [45, 90, 67]°$.

1. Introduction

Since the structure of vitamin B_{12} was determined by Hodgkin almost 50 years ago, the scientific world has been fascinated by vitamin B_{12} and the B_{12} proteins [1,2]. Although a vast body of structural and chemical information is available on the topic, many questions remain unsolved. The role of the corrin ligand and nature's choice of cobalt as the central metal is still not fully understood. The initial suggestion that an upward conformational distortion of the macrocycle can be directly linked to the enigmatic enzymatic activation of the bound coenzyme B_{12} [3] was contradicted by X-ray studies which showed no significant difference in structure between the corrinoid moiety of the coenzyme and its homolysis fragment cob(II)alamin [4]. It is still not known whether the cobalt ion is merely a spectator or if it plays an active role in B_{12} chemistry. Furthermore, different studies show that in several B_{12} proteins a 'base-off/His on' mode of binding of the corrinoid cofactor exists. In this form a histidine of the protein coordinates to the transition metal ion rather than the intramolecular dimethylbenzimidazole (DBI) base [1,2,5,6]. It is also known that

* Corresponding author. Fax: +41-1-6321538.
E-mail address: schweiger@esr.phys.chem.ethz.ch (A. Schweiger).

0009-2614/02/$ - see front matter
PII: S0009-2614(02)00521-3

the basicity of the axial ligand plays a significant role in determining the Co–C bond strength in the coenzyme, and that the basicity of the axial ligand in the Co(II) complex influences the spin density on the cobalt ion. However, to date little attention has been given to the spin density on the corrin macrocycle and its dependence on the axial ligands. To study these phenomena analytical techniques that can monitor the close vicinity of the cobalt ion are required. Electron paramagnetic resonance (EPR) is an ideal spectroscopic tool to study cob(II)alamin (or B_{12r}), the paramagnetic Co(II) form of B_{12}.

The paramagnetic species of vitamin B_{12} have been extensively studied by continuous wave (CW) EPR. For the base-on form of B_{12r} (electronic configuration $3d^7$, low-spin $S = 1/2$) the $\boldsymbol{g}$ matrix, the cobalt hyperfine interaction and the hyperfine and nuclear quadrupole interactions of the directly coordinated nitrogen of the axial DBI ligand are known from frozen solution and single-crystal measurements [7–16]. There is, however, a lack of data describing the weakly coupled ligand nuclei. Preliminary data for the remote nitrogen of the DBI ligand have recently been reported (isotropic hyperfine value $A_{iso} = 1.85$ MHz, nuclear quadrupole parameters $e^2qQ/h = 3.12$ MHz and $\eta = 0.07$) using three-pulse electron spin-echo envelope modulation (ESEEM) experiments [17]. A rough estimate was also given for the corrin nitrogen nuclei ($A_{iso} = 1.7$ MHz, $e^2qQ/h = 1.8$ MHz and $\eta = 0.85$). Thus, accurate principal values and principal axes directions of the hyperfine matrices and nuclear quadrupole tensors of the weakly coupled ligand nuclei remain unknown.

In this Letter, we report on the determination of the hyperfine and nuclear quadrupole parameters of the corrin nitrogens and the remote nitrogen of the DBI ligand using X- and Q-band hyperfine sublevel correlation (HYSCORE) [18,19] experiments.

2. Materials and methods

2.1. Sample preparation

Hydroxocob(III)alamin hydrochloride (B_{12b}) was purchased from Fluka. All solvents and liquid reagents were degassed prior to use and all procedures were carried out in a glove box. The reduction of hydroxocob(III)alamin to cob(II) alamin was achieved using the method given in [20]. A magnetically diluted powder for EPR investigations was prepared by mixing $B_{12r} : B_{12b}$ in a molar ratio of about 1:30.

2.2. Equipment

The X-band CW-EPR spectrum was measured on a Bruker ESP300 spectrometer (microwave (mw) frequency 9.45 GHz), equipped with a liquid nitrogen cyrostat. Measurements were made at 120 K with an mw power of 20 mW, a modulation amplitude of 0.1 mT, and a modulation frequency of 100 kHz. At X-band the HYSCORE spectra were recorded using a Bruker Elexsys E580 spectrometer (mw frequency 9.73 MHz). Measurements were made at 20 K with a repetition time of 1 ms.

Pulse measurements at Q-band were performed on a home-built instrument (mw frequency 35.3 GHz) [21]. The EPR spectrum was recorded by integrating the free induction decay (FID) which follows a single mw π pulse of 500 ns. Measurements were made at 20 K with a repetition time of 1 ms. The magnetic fields at both X- and Q-band were measured with a Bruker NMR ER 035M gaussmeter and calibrated with 2,2-diphenyl-1-picrylhydrazyl (DPPH, $g = 2.0036$) and the lithium phthalocyanine radical marker LiPc ($g = 2.0023$) [22]. Both pulse spectrometers were equipped with a liquid Helium cryostat from Oxford.

HYSCORE [18,19] spectra were recorded at X- and Q-band using the pulse sequence $\pi/2$–τ–$\pi/2$–t_1–π–t_2–$\pi/2$–τ-echo. An eight-step phase cycle was used to remove artifacts from unwanted echoes. At X-band the following parameters were used; mw pulses of length $t_{\pi/2} = 16$ ns and $t_\pi = 16$ ns, starting times of 96 ns for t_1 and t_2, and time increments $\Delta t = 16$ ns (data matrix 512×512). To avoid blind spots spectra were measured with τ values of 96, 158 and 208 ns. At Q-band the following parameters were used; mw pulses of length $t_{\pi/2} = 16$ ns and $t_\pi = 16$ ns, starting times of 96 ns for t_1 and t_2, and time increments $\Delta t = 8$ ns (data

matrix 350×350). To increase the modulation depth, the second and third $\pi/2$-pulses were replaced by a matched pulse of length 32 ns [23]. To avoid blind spots spectra with τ values of 96, 158, 208 and 258 ns were recorded.

2.3. Data manipulation

Data processing was done with MATLAB (The MathWorks). The HYSCORE time traces were baseline corrected using a second-order polynomial, apodized with a Hamming window and zero filled. After Fourier transformation the absolute-value spectra were calculated.

2.4. Simulation procedures

Refined **g** and cobalt hyperfine $\mathbf{A}^{\mathrm{Co}}$ matrices were obtained from the experimental CW-EPR spectra using the BRUKER WINEPR and the EASYSPIN program [24]. The simulations of the HYSCORE spectra for disordered $S = 1/2$, $I = 1$ systems were achieved using programs written in-house [25,26]. At each field position the orientations to be included in the simulation were calculated from the **g** matrix and cobalt **A** matrix. The same set of time intervals τ as in the experiments and ideal non-selective pulses were used. The Euler angles define an active rotation (right-hand) of the matrices and tensors with respect to the **g** principal axes system.

3. Evaluation of the spin hamiltonian parameters

The relevant spin Hamiltonian for a Co(II) low-spin compound in frequency units is given by

$$\mathscr{H} = (\beta_e/h)\mathbf{SgB}_0 + \Sigma\mathbf{SA}_i\mathbf{I}_i - \beta_n\Sigma g_{i,n}\mathbf{I}_i\mathbf{B}_0 + \Sigma\mathbf{I}_i\mathbf{Q}_i\mathbf{I}_i \quad (1)$$

which describes the electron Zeeman interaction, the hyperfine interactions, the nuclear Zeeman interactions and the nuclear quadrupole interactions. The CW-EPR spectrum of B_{12r} is dominated by the electronic Zeeman interaction and the hyperfine interactions with the cobalt nucleus ($I = 7/2$) and the directly coordinated nitrogen ($I = 1$) of the DBI ligand. Parameters for these interactions obtained from frozen solution and single-crystal measurements have been reported previously. The much weaker interactions of the four corrin nitrogens and the remote nitrogen of the DBI ligand are best observed with pulse EPR techniques.

The spin Hamiltonian of an $S = 1/2$, $I = 1$ subsystem can be described by the **g** matrix and the hyperfine, nuclear Zeeman and nuclear quadrupole interaction. In each of the two electron spin manifolds (α, β) three transitions between the nuclear sublevels exist (two single-quantum (sq) transitions with $|\Delta m_I| = 1$ and one double-quantum (dq) transition with $|\Delta m_I| = 2$). The **Q** tensor is traceless and the principal values are usually expressed by the nuclear quadrupole coupling constant $K = e^2qQ/4h$ and the asymmetry parameter $\eta = (Q_1 - Q_2)/Q_3$, with $Q_1 = -K(1-\eta)$, $Q_2 = -K(1+\eta)$ and $Q_3 = 2K$. In an ^{14}N HYSCORE spectrum cross-peaks may be observed between the nuclear frequencies of the α manifold and the nuclear frequencies of the β manifold.

Our analysis used X- and Q-band HYSCORE spectra. The use of two mw frequencies eliminates many ambiguities in the data analysis as the nuclear Zeeman interaction scales with the B_0 field. This allows the nuclear Zeeman interaction to be distinguished from the hyperfine and nuclear quadrupole interactions which are field independent. Additionally, Q-band HYSCORE provides improved orientational selectivity as the spectral dispersion due to **g** anisotropy scales approximately linearly with the B_0 field.

4. Results

4.1. g and A^{Co} Matrices

The EPR spectra are shown in Fig. 1, along with the simulated spectra ($g_1 = 2.272$, $g_2 = 2.230$, $g_3 = 2.004$, $A_1^{\mathrm{Co}} = 30$ MHz, $A_2^{\mathrm{Co}} = 40$ MHz, $A_3^{\mathrm{Co}} = 305$ MHz). The EPR spectra show considerable A and g strain. Fig. 2 schematically shows the orientation of the principal axes in the molecular frame defined by the g principal axes. The orientations of the $\boldsymbol{g}$ and $\boldsymbol{A}^{\mathrm{Co}}$ principal axes within the

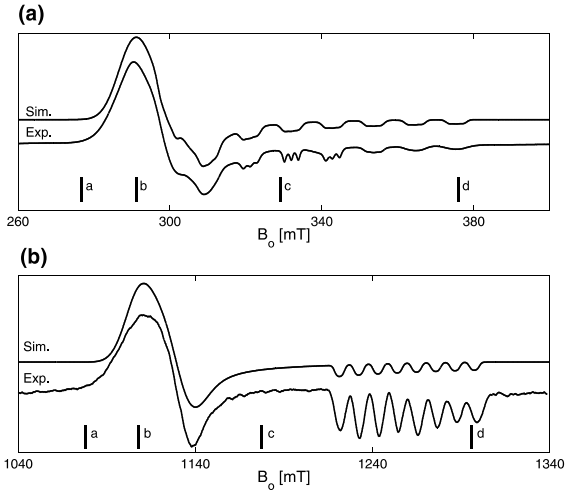

Fig. 1. EPR spectra of cob(II)alamin diluted in hydroxocob(III)alamin powder. Experimental (Exp.) and simulated (Sim.). The vertical lines indicate the observer positions of the HYSCORE spectra (note that the X-band CW-EPR and HYSCORE spectra were measured at a different mw frequency, in the figure this is taken into account): (a) X-band CW-EPR spectrum at 9.46 GHz and 120 K; (b) Q-band FID-detected EPR spectrum at 35.32 GHz and 20 K (first derivative).

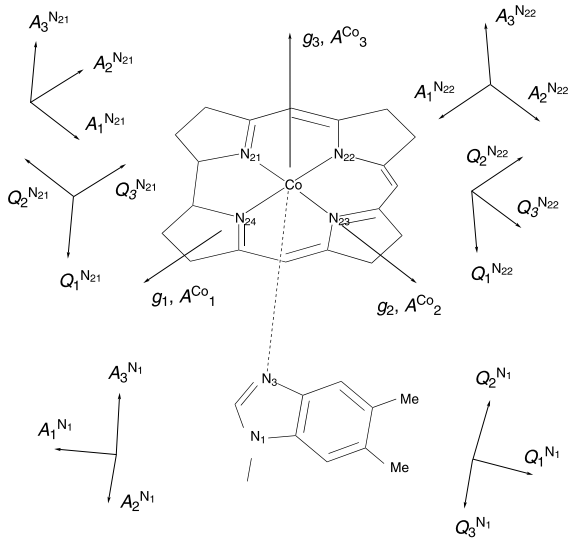

Fig. 2. Schematic representation of the principal axes of the **g** matrix, the cobalt hyperfine matrix $\mathbf{A}^{Co}$, and the nuclear quadrupole tensors **Q** and hyperfine matrices **A** of the corrin nitrogens and the remote nitrogen of the DBI ligand.

B_{12r} molecule were determined from single-crystal measurements [12].

4.2. Interactions with the four Corrin nitrogens and the remote nitrogen of the DBI ligand

Interactions of the four corrin nitrogens and the remote nitrogen of the DBI ligand were studied with HYSCORE at X-band (Fig. 3, left) and Q-band (Fig. 4, left) (for a surface plot see [27]). In both figures, the simulated spectra (right) are the sum of the corrin (four $S = 1/2$, $I = 1$ sub-systems, see later) and the remote nitrogen (one, $S = 1/2$, $I = 1$ sub-system) simulations using the parameters given in Table 1. The orientations of the hyperfine and nuclear quadrupole principal axes are shown in Fig. 2. The simulations show no combination peaks between the corrin nitrogens or between the remote nitrogen and the corrin nitrogens since only non-interacting $S = 1/2$, $I = 1$ sub-systems are considered. In Figs. 3 and 4 some of the cross-peaks have been labelled.

4.2.1. Corrin nitrogens

Single-crystal-like spectra are expected at the high-field observer positions at X- and Q-band (position *d* in Fig. 1) since only B_{12r} molecules with their $\mathbf{g}_3$ axis close to $\mathbf{B}_0$ contribute to the spectrum (calculations show that $\measuredangle(\mathbf{B}_0, \mathbf{g}_3) < 8°$). Nevertheless, the (dq_β, dq_α) transitions assigned to the corrin nitrogens produce ridges rather than narrow cross-peaks both at X-band (Fig. 3d) and at Q-band (Fig. 4d). The appearance of these ridges indicates a distribution of **A** matrices and **Q** tensors which might arise from inequivalent corrin nitrogens and/or are due to *A* and *g* strain.

At Q-band the $(dq_\beta^c, dq_\alpha^c)$ ridge is approximately perpendicular to the diagonal in the $(+,+)$ quadrant with values ranging from (4–6.5, 9.5–12 MHz). At X-band the corrin nitrogens are close to the exact cancellation condition, $|A| \cong 2\upsilon_N =$ 2.4 MHz, where *A* is the hyperfine coupling and υ_N is the nitrogen Larmor frequency, and thus the ridges occur in both quadrants. The $(dq_\beta^c, dq_\alpha^c)$ ridges have values in the range ($\pm$1.8 MHz, 4.5–6 MHz) and are approximately parallel to the υ_2 axis. Parallel ridges are observed because close to 'exact cancellation' the hyperfine and nuclear

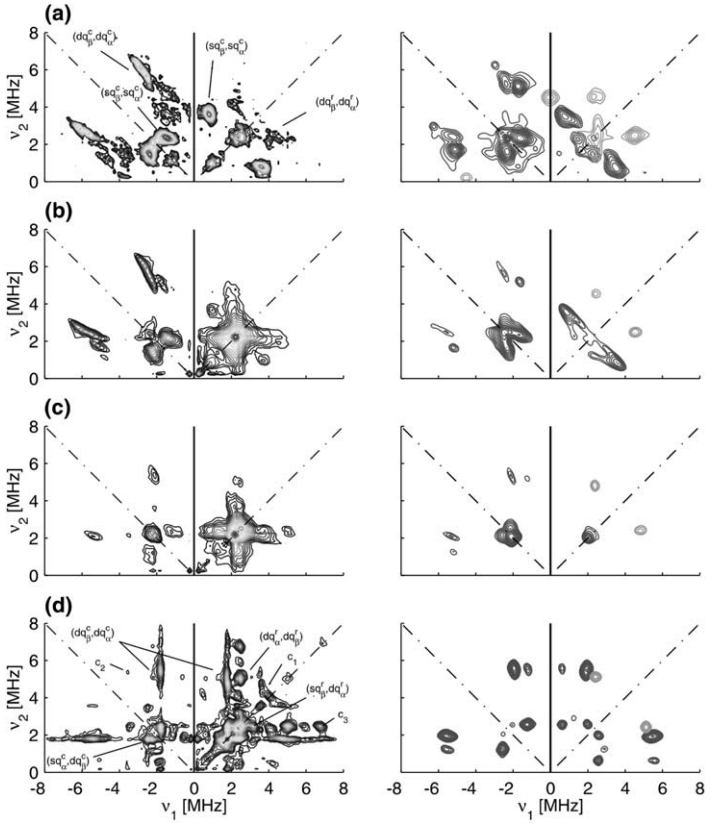

Fig. 3. X-band HYSCORE spectra at four observer positions (see Fig. 1(a)), (left) experimental, (right) simulation. Grey peaks: remote nitrogen (r) of DBI ligand, one $S = 1/2$, $I = 1$ system. Black peaks: corrin nitrogens (c), four $S = 1/2$, $I = 1$ systems. Each simulated spectrum is the sum of five non-interacting $S = 1/2$, $I = 1$ systems. Observer field positions: (a) 282 mT; (b) 298 mT; (c) 337 mT; (d) 385 mT.

Zeeman interactions are opposite in one manifold and thus partially cancel, whereas these two interactions add in the other manifold. Small changes in the hyperfine values will thus have relatively little effect on the dq frequency in one manifold, but cause relatively large changes in the dq frequency of the other manifold. The sq transitions in the α manifold produce strong cross-peaks with the dq transition in the β manifold at $(\mathrm{sq}^{\mathrm{c}}_{\alpha}, \mathrm{dq}^{\mathrm{c}}_{\beta}) = (\pm 2.3, 1.8\ \mathrm{MHz})$. There are also $(2\mathrm{dq}^{\mathrm{c}}_{\beta}, \mathrm{dq}^{\mathrm{c}}_{\alpha})$ ridges at (3.6, 4.7 MHz) and (−3.5, 5.3 MHz), which are labelled as c_1 and c_2 in Fig. 3d.

To describe the spectral features a distribution of hyperfine values along the $\mathbf{g}_3$ axis was used, as listed in Table 1. A distribution of nuclear quadrupole interactions is also expected but the resolution of the data is not sufficient to allow meaningful parameters to be determined.

At the low-field observer positions, the corrin nitrogens at both X-band (Fig. 3a) and Q-band (Fig. 4a) have peaks in the $(+,+)$ and $(-,+)$ quadrants. At these observer positions contributions stem mainly from orientations in and close to the plane spanned by the $\mathbf{g}_1$ and $\mathbf{g}_2$ axes. The observed ridges can thus originate from inequivalent corrin nitrogens and/or from equivalent nitrogens with a large hyperfine or nuclear quadrupole anisotropy in the corrin plane and/or from g and A strain. This distribution is clearly evident in the spectra, for example at X-band (Fig. 3a) the $(\mathrm{dq}^{\mathrm{c}}_{\beta}, \mathrm{dq}^{\mathrm{c}}_{\alpha})$ ridge in the $(-,+)$ quadrant with frequencies (−2.2 to −3.5, 5.2–6.7 MHz), and at

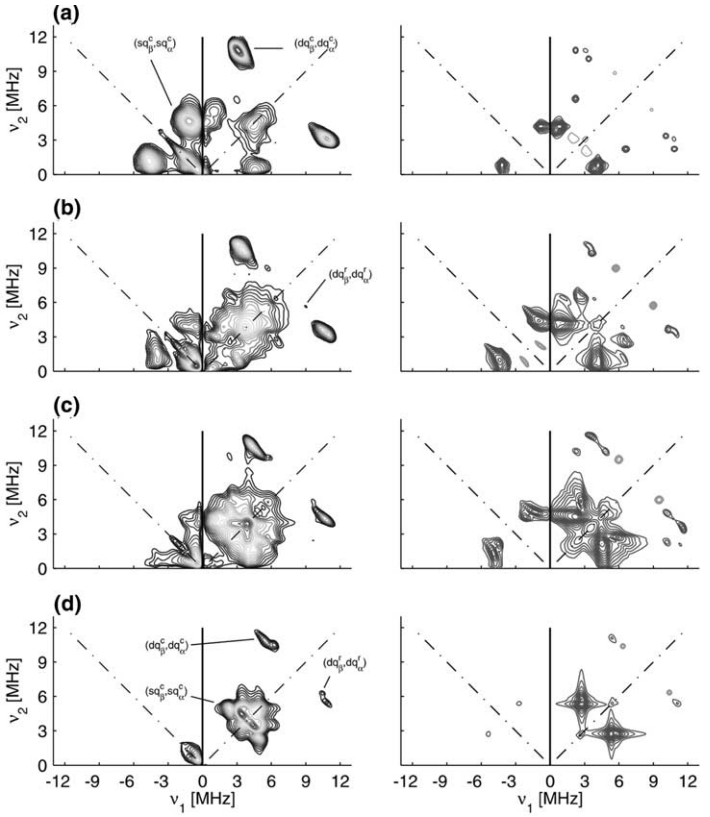

Fig. 4. Q-band HYSCORE spectra at four observer positions (see Fig. 1(b)), (left) experimental, (right) simulation. Grey peaks: remote nitrogen (r) of DBI ligand, one $S = 1/2$, $I = 1$ system. Black peaks: corrin nitrogens (c), four $S = 1/2$, $I = 1$ systems. Each simulated spectrum is the sum of five non-interacting $S = 1/2$, $I = 1$ systems. Observer field positions: (a) 1078 mT; (b) 1108 mT; (c) 1178 mT; (d) 1296 mT.

Q-band (Fig. 4a) the $(dq^c_\beta, dq^c_\alpha)$ ridge in the $(+,+)$ quadrant with frequencies (2.3–4.5, 9.5–11.8 MHz). Satisfactory simulations were obtained by assuming the corrin nitrogens have equivalent principal values (see Table 1).

4.2.2. Remote nitrogen of dimethylbenzimidazole ligand

In the X-band HYSCORE spectrum taken at the high-field observer position (Fig. 3d), the intense cross-peak between the sq and dq transition of the β manifold (at 3.1 and 5.0 MHz, respectively) and the dq transition in the α manifold (at 2.5 MHz) is ascribed to interactions with the remote nitrogen of the DBI ligand. The intense cross-peak labelled as c_3 at (6.8, 2.5 MHz) is the sum of the dq^c_β frequency of the corrin (at 1.8 MHz) and the dq^r_β frequency of the remote nitrogen (at 5.0 MHz), correlated with the dq^r_α frequency of the remote nitrogen (at 2.5 MHz), $(dq^c_\beta + dq^r_\beta, dq^r_\alpha)$. The observation of this combination peak indicates that the hyperfine coupling of the remote DBI and the corrin nitrogens have opposite signs, as combination frequencies can only occur within the same electron spin manifold. In Table 1, the corrin nitrogen hyperfine interaction is assumed to be negative (see Section 5).

At Q-band (Fig. 4d) the $(dq^r_\beta, dq^r_\alpha)$ cross-peak is observed at (10.5, 6.3 MHz). The cross-peaks between sq transitions overlap with those from the corrin nitrogens, have very low intensity and hence are difficult to identify. In the simulations they

Table 1
Hyperfine and nuclear quadrupole interactions of the corrin nitrogens and the remote nitrogen of the DBI ligand of B_{12r} and other relevant compounds

Complex/nucleus	A_1 (MHz)	A_2 (MHz)	A_3 (MHz)	$[\alpha, \beta, \gamma]$ (deg)	e^2qQ/h (MHz)	η	$[\alpha, \beta, \gamma]$ (deg)	Reference
B_{12r}/corrin	−4.5	−3.4	−2.2 to −2.5	$[n90, 25, 0]$[a]	1.75	0.95	$[90 + n90, 90, 12.5]$[a]	This work
B_{12r}/corrin	$A_{iso} = 1.7$[b]			–	1.8	0.85	–	[17]
B_{12r}/remote of DBI	1.75	1.75	2.10	$[-45, -10, 0]$	−3.3	0.10	[45, 90, 67]	This work
B_{12r}/remote of DBI	$A_{iso} = 1.85$[c]			–	3.12	0.07	[0, 70, 0][d]	[17]
Cu(II)(1, 2-dimethylimidazole)$_2$Cl$_2$/remote of 1,2-dimethylimidazole	1.70	1.24	1.18	A_3 40° from Cu–N vector[e]	−2.236	0.127	Q_3 perpendicular to imidazole group[e]	[29]
Imidazole/amino NH site	–	–	–	–	−1.391	0.930	Q_3 perpendicular to imidazole group	[30]
Benzimidazole/amino N site	–	–	–	–	−2.021	0.687	Q_3 perpendicular to imidazole plane	[30]
Co(TPP)py	−4.1	−2.9	−2.4	A_1 points along the N_{porph}–Co bond	1.8[f]	0.55	Q_3 points along the N_{porph}–Co bond	[32]
Co(dmg)$_2$(py)$_2$	2.61	1.86	1.84	A_1 points along N_{porph}–Co bond	3.4[f]	0.70	Q_3 points along the N_{porph}–Co bond	[33]

[a] $n = 0, 1, 2, 3$ for nitrogens N_{22}, N_{21}, N_{24}, N_{23}, respectively. See Fig. 2.
[b] The analysis assumed an isotropic interaction $A_{iso} = 1.7$ MHz and a point-dipole interaction with $r = 0.22$ nm (corresponding to the principal values of −0.54, −0.54 and 1.08 MHz at g_e).
[c] The analysis assumed an isotropic interaction $A_{iso} = 1.85$ MHz and a point-dipole interaction with $r = 0.3$ nm (corresponding to the principal values of −0.21, −0.21 and 0.42 MHz at g_e).
[d] The Euler angles define the mutual orientation of the **Q** tensor and **A** matrix principal axes.
[e] Single-crystal study. $\mathbf{A}_3$ axis lies 57° from the normal to the imidazole plane and 38° away from the N–C bond. The $\mathbf{Q}_3$ axis is normal to the imidazole plane and $\mathbf{Q}_2$ lies along the N–C bond and normal to the imidazole plane.
[f] Absolute value.

have insufficient intensity to be observed. Interestingly, near the $\mathbf{g}_3$ axis the signals stemming from the remote nitrogen are narrow peaks and not ridges as in the case of the corrin nitrogens. This observation may indicate that the corrin ridges observed in Figs. 3d and 4d are due to inequivalent corrin nitrogens rather than broadening due to g and A strain. At the low-field observer positions only the $(dq^r_\beta, dq^r_\alpha)$ cross-peaks have appreciable intensity. At X-band (Fig. 3a) and Q-band (Fig. 4b) they are positioned at (4.2, 2.3 MHz) and (9, 5.6 MHz), respectively.

5. Discussion

The hyperfine and nuclear quadrupole parameters determined for the remote nitrogen of the DBI ligand are collected in Table 1. The isotropic hyperfine value $A_{iso} = 1.85$ MHz reported in [17] agrees well with our data, $A_{iso} = (1.75 + 1.75 + 2.1)/3$ MHz $= 1.87$ MHz, and the anisotropy is in agreement with a point-dipole interaction [28] between the cobalt and nitrogen nucleus, $T = 0.117$ MHz, yielding $r = 0.38$ nm (X-ray value $r = 0.4$ nm). The orientation of the **A** matrix cannot be accurately determined from the powder spectra given the relatively small difference between the $A_{1,2}$ and A_3 values (0.35 MHz). Additionally, setting the $\mathbf{A}_3$ axis with the largest principal value along the Co–N vector is not a valid assumption as is demonstrated by single-crystal data from Cu(II)(1,2-dimethylimidazole)$_2$Cl$_2$ [29], where the $\mathbf{A}_3$ axis of the remote imidazole nitrogen points at 40° to the Cu–N vector (see Table 1). Our nuclear quadrupole parameters e^2qQ/h and η are similar in magnitude to those reported by [17]. The $\mathbf{Q}_3$ axis points approximately normal to the DBI plane

($\beta = 90°$). Results from NQR studies on substituted imidazoles [30] and the single-crystal ESEEM study on Cu(II)(1,2-dimethylimidazole)$_2$Cl$_2$ [29] are listed in Table 1. For Cu(II)(1,2-dimethylimidazole)$_2$Cl$_2$ the Q_3 value (there are two axial ligands with essentially the same **Q** tensors) is negative, with its axis pointing normal to the methylimidazole plane. The $\mathbf{Q}_2$ axis lies in the complex plane and points approximately along the N–CH$_3$ bond ($|Q_1| < |Q_2| < |Q_3|$). The NQR data of different substituted imidazoles [30] show that when $|e^2qQ/h|$ of the amino nitrogen is larger than 1.3 MHz, the Q_3 value is negative and its axis is perpendicular to the molecular plane, the $\mathbf{Q}_2$ axis points approximately along the N–H bond. Both these assignments are consistent with ours. Interestingly, for the substituted imidazoles when $|e^2qQ/h| < 1.3$ MHz the Q_3 value is positive and its axis lies in the molecular plane along the N–C bond.

At both X- and Q-band the corrin nitrogens produce broad ridges in the HYSCORE spectra at observer positions close to the $\mathbf{g}_3$ axis. These spectral features were described by a distribution of nitrogen hyperfine parameters along the $\mathbf{g}_3$ axis (resolution of the data is not sufficient to also include a distribution of nuclear quadrupole interactions). In the $\mathbf{g}_1$ and $\mathbf{g}_2$ directions we cannot discriminate between inequivalent corrin nitrogens or anisotropy of equivalent nitrogens. Determination of precise parameters of the four corrin nitrogens requires a single-crystal study. As listed in Table 1, the hyperfine matrices of the corrin nitrogens have the $\mathbf{A}_1$ axes (with the largest absolute coupling) pointing toward the Co ion and at 25° below the plane spanned by $\mathbf{g}_1$ and $\mathbf{g}_2$. The orientation of the principal hyperfine axes are influenced by spin density on the Co ion and the directly coordinated nitrogen of the DBI ligand. The hyperfine principal values are negative, a conclusion arrived at by the observation of combination peaks between the remote nitrogen (positive hyperfine values) and the corrin nitrogens (negative values). Further evidence in support of the assertion of negative hyperfine values comes from a series of DFT calculations on the compounds Co(II)(TPP)pyridine (TPP = tetraphenylporphyrin), Co(II)corrin with the axial ligands pyridine, 1-methylimidazole and DBI, and Cob(II)ester (heptamethyl cobyrinate) with an axial pyridine ligand. In all these compounds, the calculated hyperfine values of the nitrogens in the ring were negative and ranged between −1 and −4 MHz, an outcome consistent with our results [31].

In comparison to the porphyrin complex Co(TPP)py [32], hyperfine values of the corrin nitrogens are approximately 5% larger in magnitude but have the same sign (in the original paper the hyperfine values were assigned as positive but this has subsequently been corrected on the basis of DFT calculations [31]). The negative A_{iso} value indicates that spin polarization is the dominating contribution. The compounds Co(dmg)$_2$(pyridine)$_2$ and Co(dmg)$_2$(CH$_3$OH)$_2$ have A_{iso} values for the nitrogens of the equatorial ligands of 2.10 and 1.17 MHz, respectively [33], and provide an example where different axial ligands alter the spin density on the equatorial nitrogen ligands.

The largest nuclear quadrupole interaction Q_3 of the corrin nitrogens is positive and has its principal axis orientated in the plane of the corrin macrocycle and at 90° to the Co–N bond. Such an orientation and sign of the **Q** tensor was also found in the porphyrin complex Cu(TPP) from a single-crystal study [34] and in a σ-carbon-bonded cobalt(IV) corrin complex [35]. The $|e^2qQ/h|$ value is similar to that found for Co(TPP)py, but for B_{12r} the η is larger (0.95 as compared to 0.55).

6. Conclusion

HYSCORE measurements at both Q- and X-band provided a unique set of data which enabled the **A** matrices and **Q** tensors of the corrin nitrogens and the remote nitrogen of the DBI to be determined. The accuracy of the parameters is greatly enhanced by using two mw frequencies since this overcomes many ambiguities from the analysis of data employing a single mw frequency. At Q-band the spectral interpretation is greatly simplified since the number of combination peaks is significantly decreased. At X-band the combination peaks between different corrin nitrogens and between a corrin nitrogen and the remote nitrogen make spectral interpretation very demand-

ing and often ambiguous. Many combination peaks are observed at X-band because the hyperfine interactions are close to the exact cancellation regime, which causes strong mixing.

Our parameter determinations are based on the experimental data, results from other complexes and DFT calculations. The **A** matrix and **Q** tensor was determined for the remote nitrogen of the DBI. Many of the spectral features assigned to the corrin nitrogens, in particular the double-quantum cross-peaks, appeared as ridges. Ridges in the spectrum can result from inequivalent corrin nitrogens and/or from A and g strain. Unfortunately, the data resolution was not sufficient to confidently determine if the corrin nitrogens are inequivalent. Accurate magnetic parameters of the corrin nitrogens are of importance since they provide data relevant to understand why nature employs a corrin ring in B_{12} rather than, for example, the more symmetric porphyrin macrocycle where the four nitrogen couplings are all very similar. To obtain the individual **A** matrices and **Q** tensors of the four corrin nitrogens a single-crystal study is required. This is currently underway in our laboratory.

Acknowledgements

We are grateful to the Swiss National Science Foundation for their support.

References

[1] B. Kräutler, D. Arigoni, B.T. Golding (Eds.), Vitamin B_{12} and B_{12}-Proteins, Wiley-VCH, Weinheim, 1998.
[2] R. Banerjee, Chemistry and Biochemistry of B_{12}, Wiley, New York, 1999.
[3] J. Halpern, Science 227 (1985) 869.
[4] B. Kräutler, W. Keller, C. Kratky, J. Am. Chem. Soc. 111 (1989) 8936.
[5] E. Stupperich, H.J. Eisinger, S.P.J. Albracht, Eur. J. Biochem. 193 (1990) 105.
[6] C.L. Drennan, S. Huang, J.T. Drummond, R.G. Matthews, M.L. Ludwig, Science 266 (1994) 1669.
[7] G.N. Schrauzer, L.-P. Lee, J. Am. Chem. Soc. 90 (1968) 6541.
[8] S.A. Cockle, H.A.O. Hill, J.M. Pratt, R.J.P. Williams, Biochim. Biophys. Acta 177 (1969) 686.
[9] J.H. Bayston, F.D. Looney, J.R. Pilbrow, M.E. Winfield, Biochemistry 9 (1970) 2164.
[10] J.R. Pilbrow, M.E. Winfield, Mol. Phys. 25 (1973) 1073.
[11] E. Jörin, F. Graf, A. Schweiger, Hs.H. Günthard, Chem. Phys. Lett. 42 (1976) 376.
[12] A. Schweiger, E. Jörin, Hs.H. Günthard, Chem. Phys. Lett. 61 (1979) 223.
[13] J.R. Pilbrow, in: D. Dolphin (Ed.), EPR of B_{12}-Dependent Enzyme Reactions and Related Systems, in B_{12r}, Wiley, New York, 1982, pp. 431–462 (Chapter 12).
[14] D.N. Ramakrishna Rao, M.C.R. Symons, J. Chem. Soc. Faraday Trans. 1 (1983) 79 (see also p. 269).
[15] E. Jörin, A. Schweiger, Hs.H. Günthard, J. Am. Chem. Soc. 105 (1983) 4277.
[16] E. Shipperich, H.J. Eisiger, S.P.J. Albracht, Eur. J. Biochem. 193 (1990) 105.
[17] S.-C. Ke, M. Torrent, D.G. Museav, K. Morokuma, K. Warncke, Biochemistry 38 (1999) 12681.
[18] P. Höfer, A. Grupp, H. Nebenführ, M. Mehring, Chem. Phys. Lett. 132 (1986) 279.
[19] A. Schweiger, G. Jeschke, Principles of Pulse Electron Paramagnetic Resonance, Oxford University Press, Oxford, 2001.
[20] M. Tollinger, T. D'erer, R. Konrat, B. Kräutler, J. Mol. Catal. A 116 (1997) 147.
[21] I. Gromov, J. Shane, J. Forrer, R. Rakhmatoullin, Yu. Rozentzwaig, A. Schweiger, J. Magn. Reson. 149 (2001) 196.
[22] Ph. Turek, J.J. Andre, Sol. State Commun. 63 (1987) 741.
[23] G. Jeschke, R. Rakhmatullin, A. Schweiger, J. Magn. Reson. 131 (1998) 261.
[24] Available from http://www.esr.ethz.ch.
[25] S.A. Smith, T.O. Levante, B.H. Meier, R.R. Ernst, J. Magn. Reson. 106 (1994) 75.
[26] Z. Madi, S. Van Doorslaer, A. Schweiger, J. Magn. Reson. 181 (2002) 154.
[27] C. Calle, R.-A. Eichel, C. Finazzo, J. Forrer, J. Granwehr, I. Gromov, W. Groth, J. Harmer, M. Kälin, W. Lämmler, L. Liesum, Z. Mádi, S. Stoll, S. Van Doorslaer, A. Schweiger, Chimia 55 (2001) 763.
[28] A. Pöppl, L. Kevan, J. Phys. Chem. 100 (1996) 3387.
[29] M.J. Colaneri, J.A. Potenza, J.S. Harvey, J. Peisach, J. Am. Chem. Soc. 112 (1990) 9451.
[30] M.L.S. Garcia, J.A.S. Smith, P.M.G. Bavin, C.R. Ganellin, J. Chem. Soc. Perkin Trans. II (1983) 1391.
[31] G. Jeschke, S. Van Doorslaer, private communication.
[32] S. Van Doorslaer, R. Bachmann, A. Schweiger, J. Phys. Chem. A 103 (1999) 5446.
[33] M.D. Wirt, C.J. Bender, J. Peisach, Inorg. Chem. 34 (1995) 1663.
[34] T.G. Brown, B.M. Hoffman, Mol. Phys. 39 (1980) 1073.
[35] J. Harmer, S. Van Doorslaer, L. Gromov, M. Bröring, G. Jeschke, A. Schweiger, J. Phys. Chem. B 106 (2002) 2801.